Nanometer-Scale Resolution of Strain and Interdiffusion in Self-Assembled InAs/GaAs Quantum Dots

I. Kegel, T. H. Metzger, A. Lorke, and J. Peisl
CeNS at Sektion Physik, Ludwig-Maximilians-Universität, 80359 München, Germany

J. Stangl and G. Bauer
Institut für Halbleiterphysik, Johannes Kepler Universität Linz, A-4040 Linz, Austria

J. M. García* and P. M. Petroff
Materials Department, University of California, Santa Barbara, California 93106
(Received 19 November 1999)

Tomographic nanometer-scale images of self-assembled InAs/GaAs quantum dots have been obtained from surface-sensitive x-ray diffraction. Based on the three-dimensional intensity mapping of selected regions in reciprocal space, the method yields the shape of the dots along with the lattice parameter distribution and the vertical interdiffusion profile on a subnanometer scale. The material composition is found to vary continuously from GaAs at the base of the dot to InAs at the top.

PACS numbers: 68.65.+g, 61.10.–i

In semiconductor heterostructure systems with a few percent difference in lattice parameter between epilayer and substrate material, nanometer-sized islands may spontaneously form during growth [1–4]. While deemed to be promising candidates for future applications as quantum dots, in which electrons are confined in all three directions of space, only a few quantitative experimental data are available concerning the distribution of chemical composition and strain fields in such islands. Cross-sectional scanning tunneling microscopy has been applied successfully to determine the interdiffusion profiles of buried islands [5]. It has, however, been found that the chemical composition of uncapped islands can be different from that of the deposited material. For the deposition of $In_xGa_{1-x}As$ on GaAs, several theoretical and experimental studies have shown that, due to segregation effects, the islands' InAs content is significantly enhanced at the expense of InAs in the surrounding two-dimensional film, the so-called wetting layer [6–8]. On the other hand, if pure InAs is deposited as epilayer material, the resulting islands may consist of InGaAs: Joyce *et al.* have found evidence for alloying in uncapped InAs islands on GaAs for growth temperatures above 420 °C, and thus have suggested that significant Ga mass transport occurs [9]. Indeed recent investigations of the electronic properties indicate substantial composition gradients [10].

Hence, the determination of interdiffusion and strain profiles within quantum dots is of particular significance, both for providing target data for improved growth models explaining the microscopic mechanisms of self-organization, and also as a primary input for calculations of optoelectronic properties of quantum dots [11,12]. X-ray diffraction generally has the potential to resolve the distributions of chemical composition and strain fields [13]. In many cases, however, the complete intensity distribution has to be calculated using a structural model with a large number of free fitting parameters [14,15]. Self-assembled quantum dots, which possess an inherent wealth of three-dimensional information, call for methods providing a more direct determination of structural details.

In this paper we show that, by identifying key features of the x-ray intensity distribution in reciprocal space, one can directly reconstruct the geometry as well as the distribution of local lattice parameter and material composition. Thus, a transformation of scattering data from quantum dots to nanometer-scale tomographic images is achieved.

This transformation from reciprocal space to real space is possible for the presented class of nanostructures, provided that two fundamental conditions regarding the resolution of strain and height are fulfilled.

(i) If the lattice parameter varies monotonically by a few percent across the extent of an island whose dimensions are of the order of 10 nm [Fig. 1(a)], the intensity distribution will be spread out over a fairly large region of reciprocal space about the substrate reflection. Thus, one may think of the intensity at each point as attributed to a region of constant lattice parameter, i.e., to a slice through the quantum dot at a certain height interval. This pseudoresolution, introduced by the variation of lattice parameter [16], effectively decomposes the scattering from the dot into the contributions from its isostrain areas [Fig. 1(b)].

(ii) The dots must be free standing: the presence of a free surface around the dots serves as a reference level against which the mean height of the isostrain areas within the dots can be evaluated. At very small angles of incidence (α_i) and exit (α_f) close to the critical angle of total external reflection (α_c), the surface serves as a beam multiplier, giving rise to the four different scattering processes shown in Fig. 1(a). The diffraction process, which takes place at the isostrain area, selected by the total momentum transfer, may be combined with the two additional reflection processes before and/or after diffraction. The coherent sum of

 0031-9007/00/85(8)/1694(4)$15.00 © 2000 The American Physical Society

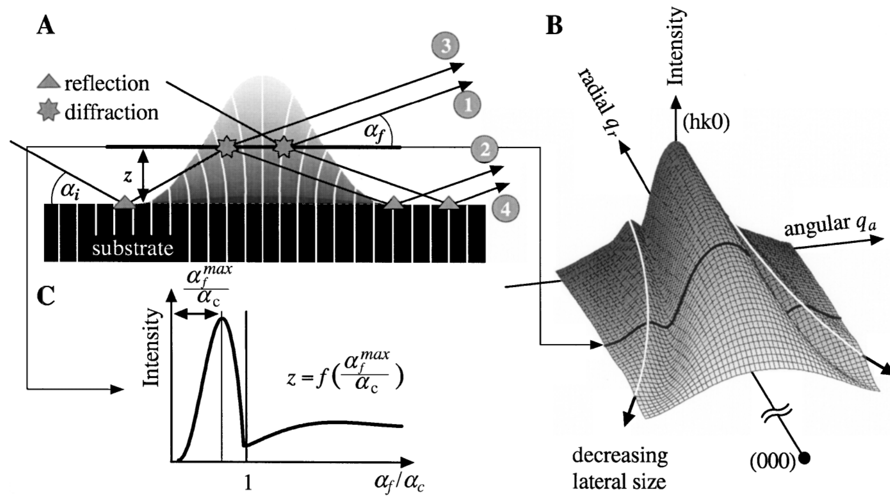

FIG. 1. Schematic representation of the method. Part (A) shows the scattering processes for a particular region of constant lateral lattice parameter at height z above the substrate (the vertical lines indicate lattice planes). The diffraction processes deflect the beam out of the plane of the paper, while reflection processes alone cannot change the azimuth of beam propagation. Angles of incidence (α_i) and exit (α_f) as well as lattice distortions are greatly exaggerated. The gray scale of the dot corresponds to a distribution of lattice parameters. A simulated intensity distribution for a section through reciprocal space close to a surface Bragg-reflection (hk0) is shown in (B). The gray scale indicates the origin of the scattered intensity in (A). The dependence of lateral extent on lattice parameter is reflected in the width of the central maximum and the positional variation of the side maxima as denoted by the white lines. Part (C) shows the simulated α_f spectrum corresponding to the isostrain area at the selected height z (α_c is the critical angle of total external reflection). The numerical value of z is calculated from the maximum position $\alpha_f^{\max}$.

these four amplitude terms causes distinct features in the spectra along the exit angle (α_f), from which the mean height above the substrate can be directly calculated with sub-nm accuracy [Fig. 1(c)].

Here, we present the results obtained from self-assembled InAs islands, grown by solid source molecular beam epitaxy on GaAs(001). A total of 1.9 ML (monolayers) of InAs (7% lattice mismatch with respect to GaAs) was deposited at a substrate temperature of 530 °C. In and As were deposited alternately: the In shutter was opened for 4 s, followed by a growth interruption of 2 s under an As beam equivalent pressure of 1×10^{-5} Torr. One such cycle resulted in a deposition of 0.15 ML of InAs. The transition from 2D to 3D growth was observed *in situ* by reflection high energy electron diffraction at 1.7 ML. As shown by atomic force microscopy [17], the chosen growth conditions lead to rotationally symmetric quantum dots, with a random lateral arrangement of dot positions. Transmission electron microscopy investigations on the dots clearly showed no evidence for dislocations, as expected for these growth parameters.

Measurements are performed in a grazing incidence diffraction setup [18] at ambient conditions. By choosing an incident angle in the total reflection regime below α_c, the penetration depth of the evanescent x-ray beam is of the order of 5–10 nm [19], maximizing the relative scattering power of the dots with respect to the substrate. As a consequence of the diffraction geometry, only the crystalline core of the dots is considered. A comparison with forward scattering experiments shows that the average thickness of the oxide layer on the dots is less than 1 nm. All measurements have been performed at the TROÏKA II beam line at the European Synchrotron Radiation Facility in Grenoble at a wavelength of 1.5 Å. In order to determine the three-dimensional structure of the dot, both geometry and strain field are extracted from a three-dimensional intensity map of reciprocal space between the (220) surface Bragg reflections of GaAs and InAs. At each radial position q_r, as defined in Fig. 1(b), a two-dimensional reciprocal space map is analyzed in four steps (Fig. 2).

(i) The lateral extent of the isostrain area, selected by the choice of q_r, is calculated from the width of the central peak (Δq_a) in an angular slice at low α_f [16].

(ii) The α_f spectrum at zero angular position as shown in Fig. 1(c), reveals the height above the surface of the isostrain area. From the position $\alpha_f^{\max}$ of the pronounced maximum, the height z can be calculated in a straight forward manner as [20]

$$z = \frac{1}{k\alpha_f^{\max}} \arccos \frac{\alpha_f^{\max}}{\alpha_c}, \quad (1)$$

where k is the wave number of the x-ray beam and α_c is the critical angle of the GaAs substrate. Figure 3 shows the experimental α_f spectra with corresponding simulations of the four-process scattering functions, which extend the transmission functions of grazing incidence diffraction to the more general case of a three-dimensionally structured surface. The prominent peak, signified by the dark dots, is usually referred to as the "Yoneda peak," which appears at

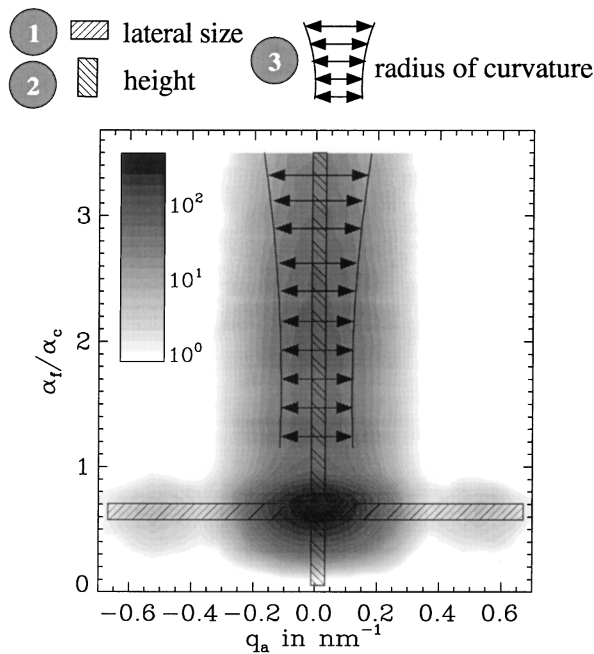

FIG. 2. Data analysis for a measured reciprocal space map in the q_a-α_f plane at $q_r = 1.17\ \mathrm{nm}^{-1}$. The lateral size of the strain state selected by q_r is extracted from the intensity distribution along the horizontal slice (1). Analysis of the vertical slice yields the mean height above the substrate (2). The radius of curvature is extracted from the dependence of the half widths in q_a on α_f/α_c (3).

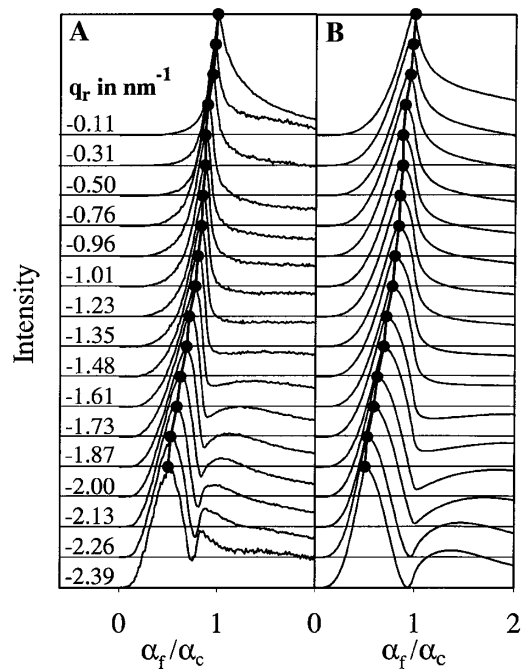

FIG. 3. Comparison of experimental α_f spectra (A) with the corresponding simulated four-process-scattering functions for flat isostrain areas (B) showing the same shift of the maximum α_f positions.

α_f (or α_i) $= \alpha_c$ for the usual case of a flat surface. The shift of the Yoneda peak to lower angles for increasing q_r, used to determine the height z above the substrate, is well reproduced by the theory.

(iii) In order to obtain the bending of the isostrain area, its mean radius of curvature is evaluated by comparing the dependence of angular half widths on α_f (see Fig. 2) with simulations of a suitably curved isostrain area. In our case of rotationally symmetric dots, we use segments of hollow spheres with lateral extents taken from the first step. The resulting shape of the dots obtained after these first three steps agrees with atomic force microscopy images.

(iv) Comparing the intensity distributions from a strong and a weak reflection along a common azimuth, we can additionally determine the InAs content, i.e., the vertical interdiffusion profile within the dot. For a strong reflection, such as (400), the intensity is determined by the square of the sum of the atomic form factors of Ga and As or In and As, whereas for the (200) reflection the scattered intensity scales as the square of the difference of these form factors [21]. With Ga and As being only two electrons apart, the (200) reflection of GaAs is extremely weak, whereas for InAs it is appreciable. Extended to an $In_xGa_{1-x}As$ alloy, the ratio of the intensities at the strong and weak reflections at a particular radial position determines the Ga content in the vicinity of the selected isostrain area. Note that no information is available as for the lateral variation in composition, but only the mean InAs content for different strain states can be resolved.

By combining all of the information derived in steps (i)–(iv), we obtain the distribution of strain and material composition within the island (Fig. 4), averaged for the entire ensemble of dots in the area which is selected by the scattering geometry ($\approx 1\ \mathrm{mm}^2$). The interdependence of shape and strain field is shown in Fig. 4(a), where the lateral lattice parameter varies from that of pure GaAs at the bottom of the dot to the lattice constant of pure InAs at its top. Figure 4(b) shows the Ga content x of the $In_{(1-x)}Ga_xAs$ alloy as a function of strain ranging from close to 100% at the bottom to 0% at the top with a remarkably large fraction of Ga in the dot center. Contributions from the GaAs substrate due to tensile strain are thus very weak, which is also inferred from the low scattering intensity of compressive strain components at positive q_r, which would be strong in the presence of large tensile strains.

Several recent experiments [7,9,22,23] suggest that the conventional picture of Stranski-Krastanow growth may be too simple, and strong dependencies of the growth mode on growth parameters such as temperature, flux rates, and flux ratios [24–26] have been reported. With our method we can quantitatively determine the composition and strain profiles of free-standing quantum dots.

The *in-plane* strain distribution shown in Fig. 4(a) results exclusively from the experimentally determined curvature of the isostrain areas. Similarly, we do not have

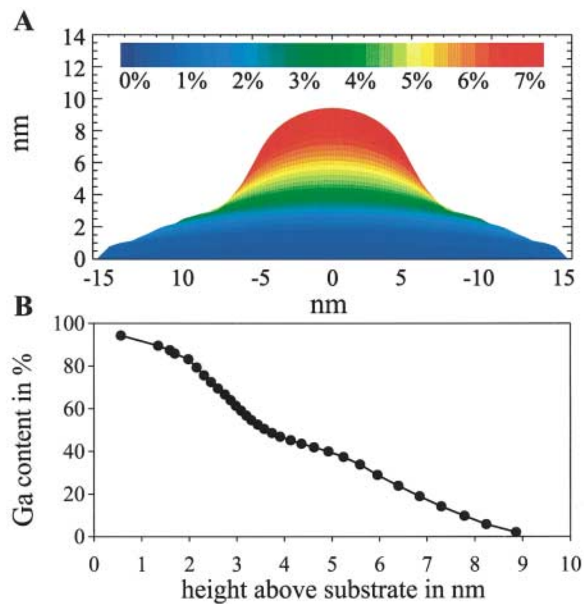

FIG. 4 (color). Experimental results for the InAs/GaAs dot system. (A) shows the deviation of lateral lattice parameter from that of GaAs, whereas in (B) the Ga-content x of the $In_{(1-x)}Ga_xAs$ alloy is displayed as a function of height above the substrate.

any *direct* way of determining a possible lateral variation in composition, as found recently by Liu *et al.* [5], who deposited $In_{0.5}Ga_{0.5}As$. Atomistic calculations of strain relaxation based on semiclassical potentials show, however, that the determined strain distribution in our sample is self-consistent with a laterally homogeneous composition, but *not* with an "inverted-cone In-profile" as found in Ref. [5] for *buried* islands. Likewise, also finite element calculations show that the measured strain distribution [Fig. 4(a)] is consistent with the measured interdiffusion profile [Fig. 4(b)], but not with a dot of pure InAs. Thus we believe that the reduction of elastic energy is the main driving force for alloying of the dot, although the particular interdiffusion profile might depend very sensitively on the actual growth parameters. Consequently, although our method gives no *direct* lateral spatial resolution in the sub-nm range, combining the measurements of height, radius, and curvature of the isostrain areas, and taking symmetry considerations into account, we are able to reconstruct the strain and composition distribution in the dots.

In conclusion, the presented technique allows for the determination of strain distribution and interdiffusion profile within the free-standing InAs dots. The accessibility of the internal structure of self-assembled quantum dots is a key prerequisite for the verifiability of microscopic growth models. In addition, it delivers experimental input to calculations of electronic and optical properties.

We thank K. Nordlund for his swift support with the atomistic calculations and D. Smilgies for the excellent conditions at the TROÏKA II beamline at the European Synchrotron Radiation Facility. This work was supported by the Deutsche Forschungsgemeinschaft under Grant No. Pe 127/1-6+2.

---

*Present address: Instituto de Microelectronica de Madrid (CNM/CSIC), Isaac Newton 8, 28760, Tres Cantos, Madrid, Spain.

[1] MRS Bull. **23**, No. 2 (1998).
[2] S. Guha, A. Madhukar, and K. C. Rajkumar, Appl. Phys. Lett. **57**, 2110 (1990).
[3] R. Leon *et al.,* Science **267**, 1966 (1995).
[4] A. P. Alivisatos, Science **271**, 933 (1996).
[5] N. Liu *et al.,* Phys. Rev. Lett. **84**, 334 (2000).
[6] J. Tersoff, Phys. Rev. Lett. **81**, 3183 (1998).
[7] N. Grandjean, J. Massies, and O. Tottereau, Phys. Rev. B **55**, R10189 (1997).
[8] X. Z. Liao *et al.,* Phys. Rev. Lett. **83**, 1273 (1999).
[9] P. B. Joyce *et al.,* Phys. Rev. B **58**, R15981 (1998).
[10] P. W. Fry *et al.,* Phys. Rev. Lett. **84**, 733 (2000).
[11] F. H. Julien and A. Alexandrou, Science **282**, 1429 (1998).
[12] D. Bimberg, M. Grundmann, and N. N. Ledentsov, *Quantum Dot Heterostructures* (Wiley, Chichester, 1999).
[13] Q. Shen, C. C. Umbach, B. Weselak, and J. M. Blakely, Phys. Rev. B **53**, R4237 (1996).
[14] A. J. Steinfort *et al.,* Phys. Rev. Lett. **77**, 2009 (1996).
[15] M. Schmidbauer *et al.,* J. Phys. D **32**, A230 (1999).
[16] I. Kegel *et al.,* Europhys. Lett. **45**, 222 (1999).
[17] J. M. García *et al.,* Appl. Phys. Lett. **71**, 2014 (1997).
[18] T. Salditt *et al.,* Phys. Rev. B **51**, 5617 (1995).
[19] M. Tolan, *X-Ray Scattering from Soft-Matter Thin Films* (Springer-Verlag, Berlin, 1999), Chap. 2.
[20] The complete derivation of Eq. (1) will be given in a future publication.
[21] B. E. Warren, *X-Ray Diffraction* (Dover, New York, 1990), Chap. 3.3.
[22] E. Mateeva, P. Sutter, and M. G. Lagally, Appl. Phys. Lett. **74**, 567 (1999).
[23] G. Medeiros-Ribeiro *et al.,* Science **279**, 353 (1998).
[24] A. Madhukar, Q. Xie, P. Chen, and A. Konkar, Appl. Phys. Lett. **64**, 2727 (1994).
[25] G. S. Solomon, J. A. Trezza, and J. S. Harris, Appl. Phys. Lett. **66**, 991 (1995).
[26] H. Eisele *et al.,* Appl. Phys. Lett. **75**, 106 (1999).